Lawrence Berkeley National Laboratory
Recent Work

Title
MATHEMATICAL MODELING OF LiAl/LiCl, KCl/FeS CELLS

Permalink
https://escholarship.org/uc/item/1583n3zs

Authors
Bernardi, D.
Pawlikowski, E.M.
Newman, J.

Publication Date
1986-11-01

Lawrence Berkeley Laboratory
UNIVERSITY OF CALIFORNIA

Materials & Molecular Research Division

MAR 1 7 1987

MATHEMATICAL MODELING OF LiAl/LiCl,KCl/FeS CELLS

D. Bernardi, E.M. Pawlikowski, and J. Newman

November 1986

DISCLAIMER

Mathematical Modeling of LiAl/LiCl,KCl/FeS Cells

Dawn Bernardi,[1] Ellen M. Pawlikowski,[2] and John Newman

Materials and Molecular Research Division,
Lawrence Berkeley Laboratory, and
Department of Chemical Engineering,
University of California,
Berkeley, California 94720

November 24, 1986

Abstract

The behavior of the thermodynamic, open-circuit potential of the LiAl/LiCl,KCl/FeS cell as a function of state of charge and temperature is investigated. A thermodynamically consistent set of expressions for the open-circuit potential is presented. A nonequilibrium computer model is presented, and results are focused on the case with $LiK_6FeS_{24}S_{26}Cl$ as the intermediate discharge product of the FeS electrode. The model is used to predict the cell voltage and LiCl composition throughout the cell during discharge. The results of the predicted cell voltage behavior during discharge compare favorably with available experimental data. The effect of KCl precipitation on positive-electrode utilization is discussed. Agreement between experimental and predicted maximum utilization can be achieved only by consideration of expansion of the positive electrode.

Key words: Cell model, high-temperature battery, molten salt.

[1]Present address: General Motors Research Laboratories, Warren, Michigan 48090-9055.

[2]Present address: Air Force Technical Application Center, Patrick Air Force Base, Florida 32925-6001.

Introduction

Lithium aluminum, iron sulfide cells were conceived for electric vehicle propulsion and energy storage applications.[1] The melting point of the electrolyte in these cells usually restricts the operating temperatures to above 400°C. The advantages of using a molten-salt electrolyte over an aqueous electrolyte include reducing electrolyte decomposition, ohmic resistance, and mass-transfer limitations. High temperature operation also promotes relatively fast electrode reactions compared to cells operated at lower temperatures. The disadvantages of operating at high temperatures are increased corrosion of cell components and increased volatility and solubility of active material.[2] In terms of engineering development, the LiAl/FeS cell is currently the most technically advanced system of this type. An extensive compilation of state-of-the-art LiAl/FeS cell design, construction, and performance has been published by Gay *et al.*[1]

During the discharge of an FeS electrode in LiCl-KCl electrolyte, investigators have identified two intermediate sulfide phases, X-phase (Li_2FeS_2) and J-phase ($LiK_6Fe_{24}S_{26}Cl$).[3] The thermodynamic behavior of LiAl/FeS cells in LiCl-KCl electrolyte involves these intermediates and is investigated in the first part of this paper.

A mathematical model of the LiAl/LiCl-KCl/FeS cell with X-phase as the intermediate in the positive electrode was developed by Pollard and Newman[4,5,6] in 1979. Much of their work was done in conjunction with experimental investigations at Argonne National Laboratory. Pollard and Newman predicted regions of bipolarity within the electrodes under certain operating conditions. The understanding of bipolar regions observed in experimental LiAl electrodes[7,8] was facilitated by Pollard and

Newman's model results. Pollard and Newman predict LiCl precipitation in the LiAl electrode and KCl precipitation in the FeS electrode during discharge under certain operating conditions. Precipitation is also observed experimentally during discharge.[3,7] Pollard and Newman's model predicts that the clogging of pores by KCl precipitation is the primary capacity-limiting mechanism of these cells. The galvanostatic discharge behavior constitutes the main emphasis of our work. Pollard and Newman discuss the relaxation and charge behavior in Reference 6.

The results of the modeling work for the LiAl/FeS cell subsequent to the original work of Pollard and Newman are presented in the second part of this paper. The model developed by Pollard and Newman incorporates only the X-phase intermediate. In this work, the galvanostatic discharge behavior of a model with J-phase as the intermediate in the positive electrode is presented, and the effect of KCl precipitation on positive-electrode utilization is examined. The formation of J-phase during discharge is undesirable because of the lack of reversibility of reactions involving J-phase.[3] This will be discussed in greater detail later.

Thermodynamic Behavior of LiAl/FeS Cells

An understanding of the thermodynamic behavior of LiAl/FeS cells can aid in the development and design of these cells. A large research effort has been directed toward the understanding of the chemistry of the FeS electrode in molten LiCl-KCl electrolyte. This successful endeavor is reviewed extensively by Selman and Saboungi.[3] Much of the success of this research may be attributed to the work done at Argonne National

Laboratory.

Tomczuk *et al.*[9] present a thermodynamic analysis of the FeS electrode with broad scope, utilizing a number of experimental techniques. The researchers combined EMF and cyclic voltammetric measurements with metallography and x-ray diffraction results to characterize the electrode. Photomicrographs of coexisting electrode phases are shown, and complex reaction sequences are identified. The authors also discuss the chemical reactions that can occur if regions of an electrode are not equilibrated.

The LiAl electrode material is a two-phase alloy and is well understood. The lithium activity of lithium-aluminum is constant between approximately 8 and 49 atom percent lithium, where the two phases, α and β, coexist.[2] The potential of the LiAl electrode in LiCl-KCl electrolyte at 400°C is approximately 300 mV positive to that of liquid lithium. The β-LiAl is 47.5 atom percent lithium, and the α phase is 10 percent. The reaction of this electrode during discharge is

$$\text{LiAl}(\beta \text{ - phase}) \rightarrow \text{Li}^+ + \text{Al}(\alpha \text{ - phase}) + e^- \, .$$
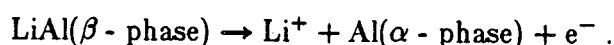
In this section, we summarize and extend some of the important findings of the work of Tomczuk *et al.* The results of Tomczuk *et al.* allow the determination of the thermodynamic behavior of a LiAl/FeS cell that is operated in an infinite amount of electrolyte. We have extended their analysis to give the behavior of a cell with a finite amount of electrolyte at any initial composition.

The Regions of Stability of FeS in LiCl-KCl Electrolyte.—There are five compounds that have been identified during the discharge of an FeS electrode. These compounds are: FeS, Li_2S, Fe, Li_2FeS_2 (X-phase), and $LiK_6Fe_{24}S_{26}Cl$ (J-phase). FeS is the original

electrode material, and Li_2S and Fe are the products of complete discharge. The intermediate phases formed during discharge are referred to as J-phase and X-phase. Three independent electrochemical reactions can be written for this system. Table 1 gives five electrochemical reactions that we use to describe the FeS electrode. (Only three of the reactions are used at a given temperature.) Each reaction involves two sulfide phases and Fe. The Gibbs phase rule can be applied at a given temperature to show that there is only one degree of freedom for reactions 3 and 4, and two degrees of freedom for reactions 1, 2, and 5; hence, electrode reactions 3 and 4 are characterized by constant open-circuit potentials relative to the $(\alpha\text{-}\beta)$ LiAl reference electrode (at constant temperature and pressure), and reactions 1, 2, and 5 have potentials that vary with electrolyte composition. In the remainder of this section, the primary data needed to describe the ther-

Table 1. Electrochemical Reactions of the FeS electrode.

1. $26FeS + Li^+ + Cl^- + 6K^+ + 6e^- \rightarrow LiK_6Fe_{24}S_{26}Cl + 2Fe$

    (J-phase)

2. $J + 25Li^+ + 20e^- \rightarrow 13Li_2FeS_2 + 11Fe + 6K^+ + Cl^-$

    (X-phase)

3. $2FeS + 2Li^+ + 2e^- \rightarrow Li_2FeS_2 + Fe$

4. $Li_2FeS_2 + 2Li^+ + 2e^- \rightarrow 2Li_2S + Fe$

5. $J + 51Li^+ + 46e^- \rightarrow 26Li_2S + 24Fe + 6K^+ + Cl^-$
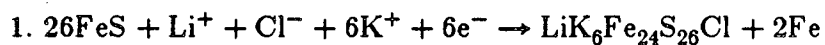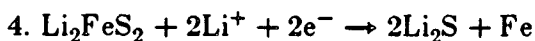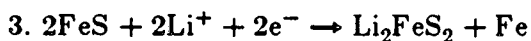
modynamic behavior of this system and the possible reaction sequences during the discharge of a LiAl/FeS cell are discussed.

The thermodynamic, open-circuit potential data at a single electrolyte composition (eutectic in this case) and electrolyte activity coefficient data for a range of compositions are referred to as *primary data*. We can use these primary data to calculate the thermodynamic, open-circuit potential for a range of compositions. The primary, open-circuit potential data are given for the eutectic composition of the electrolyte as a reference condition and are of the form

$$U_{l,eut} = a_l + b_l T .$$
(1)

Table 2 gives the literature data for the coefficients in this equation, corresponding to the five reactions in Table 1. Equation 1 yields the potential in volts and requires the temperature in kelvins. All the electrode reaction potentials are given relative to the two-phase (α, β) LiAl alloy reference electrode.

The poor reversibility of the electrochemical reactions involving J-phase leads to large uncertainties in the determination of their thermodynamic properties.[9] As we mentioned earlier, only three of the reactions are independent, so the thermodynamic data for reactions 1 and 5 are calculated from data for reactions 2, 3, and 4. The second entries for reactions 1 and 5 have the parameters calculated in this manner. The differences between the calculated and the experimental data for reactions 1 and 5 indicate that the original data are thermodynamically inconsistent. The consistent data are used in our thermodynamic calculations.

Table 2. Coefficients for the Open-Circuit Potential.

Reaction	a_l	$b_l \times 10^3$
	[V]	[V/K]
1.	1.9547[9]	-0.68[9]
1.‡	1.8328	-0.5267
2.	1.19072[9]	-0.1753[9]
3.	1.3389[10]	0.0133[10]
4.	1.43211[10]	-0.147[10]
5.	1.33978[9]	-0.02445[9]
5.‡	1.3272	-0.0068696

‡Recalculated to be thermodynamically consistent
with the literature values for reactions 2, 3, and 4.

The activity-coefficient data were obtained from Reference 11, and can be fit as functions of composition by the equations

$$T \ln \gamma_{LiCl} = 723.15 \left(0.52628 x_{KCl} - 1.2738 x_{KCl}^2 - 2.9783 x_{KCl}^3 \right)$$

and

$$T \ln \gamma_{KCl} = 723.15 \left(-0.52628 x_{LiCl} - 5.7413 x_{LiCl}^2 + 2.9783 x_{LiCl}^3 - 0.52628 \ln x_{KCl} \right) .$$

The activity coefficients γ_{LiCl} and γ_{KCl} are written without regard for their dissociation.

The theoretical, open-circuit potential for reaction l as a function of electrolyte composition, relative to a reference electrode in the same solution, is written as

$$U_l = U_l^o - U_{RE}^o + \frac{RT}{n_{RE} F} \sum_i s_{i,RE} \ln(a_i) - \frac{RT}{n_l F} \sum_i s_{i,l} \ln(a_i). \qquad (2)$$

The stoichiometric coefficients are negative for cathodic reactants and positive for anodic reactants. The ionic species i are Li^+, K^+, and Cl^-. For the case of the LiAl/FeS cell, it is convenient that the negative electrode is the same material as the reference electrode. Equation 2 can be applied to the FeS electrode in LiCl-KCl electrolyte to relate U_l to $U_{l,eut}$:

$$U_l = U_{l,eut} - \frac{RT}{F} \ln \left[\left[\frac{x_{Li^+} \gamma_{LiCl}}{x_{Li^+}^{eut} \gamma_{LiCl}^{eut}} \right]^{\frac{s_{Li^+,l}}{n_l} - \frac{s_{Li^+,RE}}{n_{RE}}} \left[\frac{x_{Cl^-}}{x_{Cl^-}^{eut}} \right]^{\frac{-s_{Cl^-}}{n_l}} \left[\frac{x_{K^+} \gamma_{KCl}}{x_{K^+}^{eut} \gamma_{KCl}^{eut}} \right]^{\frac{s_{K^+,l}}{n_l}} \right]. \qquad (3)$$

The relative activities of LiCl and KCl are defined as $x_{LiCl} \gamma_{LiCl}$ and $x_{KCl} \gamma_{KCl}$, respectively. The open-circuit potentials of reactions 1, 2, and 5 can be written easily in terms of electrolyte activity to yield potentials at any composition with this equation. As an example, the substitution of primary data into Equation 3 for reaction 1 will be described. The stoichiometric coefficients for reaction 1, a_1 and b_1, from Table 2, and the activity at eutectic composition ($x_{LiCl}^{eut} = 0.58$) can be substituted into Equation 3 to give

$$U_1 = 2.0178 - 0.6444 \times 10^{-3} T -$$

$$\frac{RT}{F} \left[\frac{5}{6} \ln \left(x_{LiCl} \gamma_{LiCl} \right) - \ln \left(x_{KCl} \gamma_{KCl} \right) \right]. \qquad (4)$$

Equation 3 also gives the thermodynamic, open-circuit potential for LiCl-KCl electrolytes that contain inert compounds. For example, this equation yields the thermodynamic, open-circuit potential of a LiAl/FeS cell with LiCl-KCl-LiF electrolyte. $x_{Li^+} = \frac{1}{2}(x_{LiCl} + x_{LiF})$, $x_{K^+} = \frac{1}{2}(x_{KCl})$, and $x_{Cl^-} = \frac{1}{2}(x_{LiCl} + x_{KCl})$ are substituted into Equation 3 to yield the correct open-circuit potential if γ_{LiCl} and γ_{KCl} for the LiCl-KCl-LiF system are known.

Material balances can be written to relate the electrolyte composition to the state-of-discharge. We define two parameters of importance: the initial composition of electrolyte x^o_{LiCl} and the initial number of moles of electrolyte per mole of FeS, n^o_e. In Reference 12 we compare thermodynamic, open-circuit potential calculations from Equation 3 (and the data in Table 2) to experimental data (Reference 13) of LiAl/LiCl-KCl/FeS cells. The calculated voltages agree with the experimental results to within a few millivolts for most of the data. (There are large discrepancies at 0% utilization, and possible reasons for this are discussed in Reference 12.)

Figure 1 gives a plot of temperature versus state-of-discharge showing the regions in which reactions 1 through 5 occur. The state-of-discharge is put in terms of utilization of FeS. Utilization is defined as the ratio of charged passed to the total charge available in the positive electrode if it were discharged to Li_2S and Fe.

This plot gives the reaction sequences during equilibrium discharge of a LiAl/FeS cell and can give insight into the different discharge mechanisms possible during cell operation. The initial conditions are for a cell being discharged with a eutectic composition of electrolyte and an electrolyte to FeS ratio of 1.0. The numbers within the designated regions refer to the reactions that are thermodynamically possible. First let us
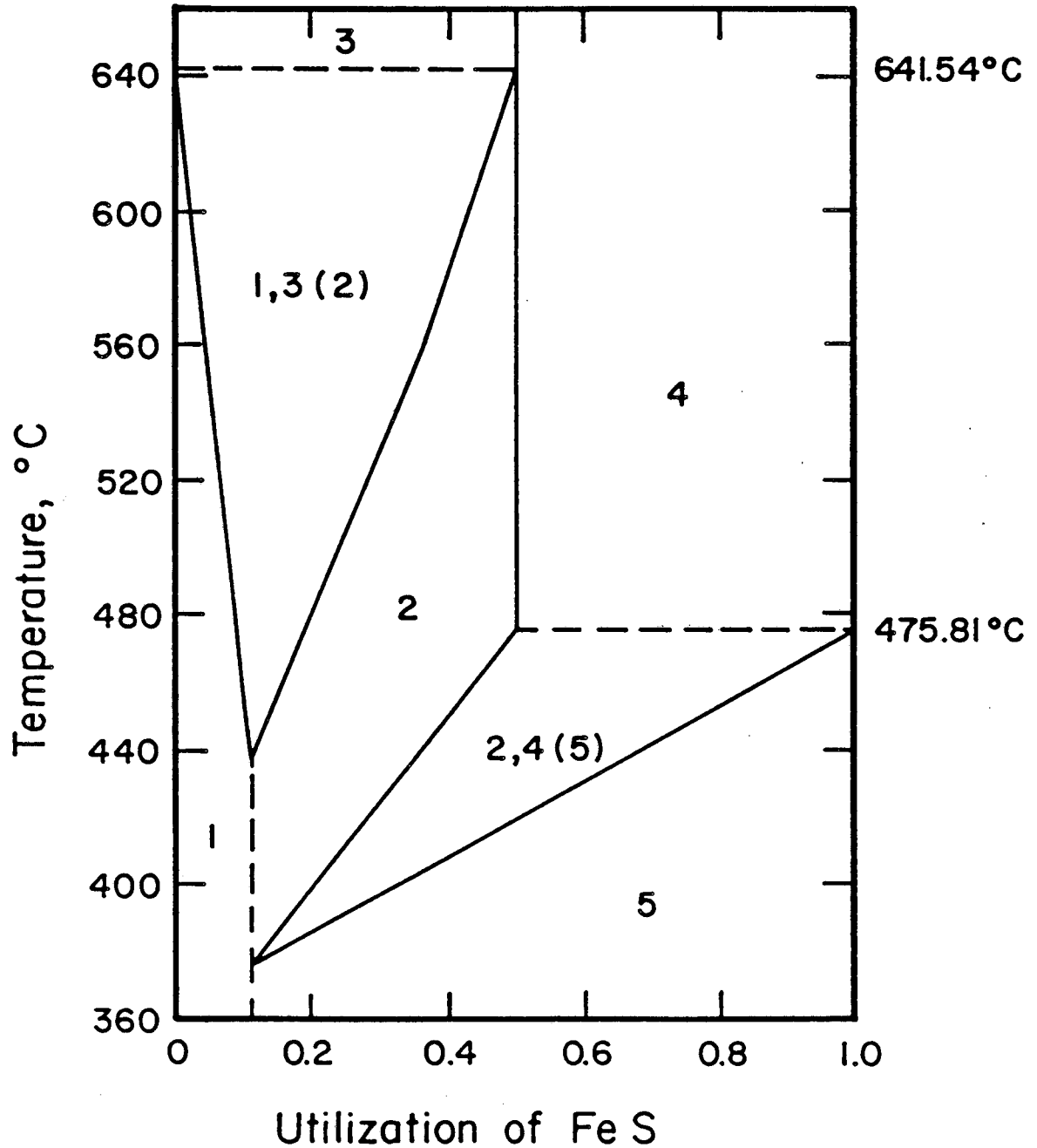
Figure 1. Reaction regions as a function of temperature and utilization for a cell with $x^o_{LiCl} = 0.58$ and $n^o_e = 1.0$. The numbers refer to the reactions in Table 1, and parentheses indicate a reaction that can be obtained from the other two reactions.

describe this figure in the context of an isothermal cell discharge. As discharge proceeds at a temperature below 641.5°C, the first reaction (FeS to J-phase) causes the electrolyte composition to shift by depleting the KCl species. Reaction 1 alone occurs to a utilization that is defined by the boundary of the region of reaction 1, and is less than 11.5%. If the temperature is greater than 440°C, the upper triangular region is entered as discharge continues. Five phases are equilibrated in this region: FeS, J-phase, X-phase, Fe, and the electrolyte phase. Upon entering this region, X-phase begins to form (reaction 2), and the electrolyte composition stabilizes until the FeS is exhausted. One could say that reaction 3 alone occurs in this region (reaction 1 plus reaction 2), since this reaction leaves the composition stationary. The exhaustion of FeS is marked by the utilization at the right side of the upper triangle, and is less than 50%.

After exhaustion of FeS, reaction 2 occurs (J-phase to X-phase), and this shifts the composition back toward eutectic. If the temperature is below 475.8°C and greater than about 377°C, the lower triangular region is entered as discharge proceeds. In this region, five phases (J-phase, X-phase, Li_2S, Fe, and the electrolyte) are equilibrated. X-phase reacts to Li_2S (reaction 4), and the composition will remain constant until X-phase is exhausted. The X-phase is exhausted at the utilization defining the right side of the lower triangular region. In the final region of discharge, the remaining J-phase reacts to Li_2S and Fe (reaction 5), and the composition will continue its downward shift toward eutectic.

If the temperature is greater than 475.8°C, the lower triangular region is not entered during discharge. Instead, the region in which reaction 2 occurs is entered, and

the J-phase is exhausted at 50% utilization. Reaction 4 begins at 50% utilization, and X-phase reacts to Li_2S and Fe. In this final region of discharge, three phases are equilibrated: X-phase, Li_2S, and Fe.

If the temperature is greater than 641.5°C, J-phase never becomes stable. FeS reacts to X-phase (reaction 3) from 0 to 50% utilization, and from 50 to 100% utilization, X-phase reacts to Li_2S (reaction 4). We call this the X-phase mechanism.

If the temperature is below about 377°C, X-phase will not form, and the reaction sequence is FeS to J-phase (reaction 1) from 0 to 11.5% utilization, followed by J-phase to Li_2S and Fe (reaction 5) from 11.5 to 100% utilization. We call this the J-phase mechanism. The X-phase and J-phase mechanisms are simple compared to the reaction sequences that are possible in the temperature range from 641.5 to 377°C for the conditions of Figure 1. Only mathematical model results with the J-phase mechanism are presented in this work.

The boundaries designated in Figure 1, which define the reaction sequences, are a function of the initial composition and the amount of electrolyte. If the amount of electrolyte is increased, the size of the the two triangular shaped regions will decrease. The dashed sides of the triangles will remain in place. The bottom tips of the triangles will remain at 11.5% utilization, but tips of the upper and lower triangles will shift toward 641.5 and 475.8°C, respectively. As the amount of electrolyte approaches infinity, the triangles become infinitely thin. In this limiting case, there are only three possible reaction sequences: the X-phase mechanism; the J-phase mechanism; and three reaction sequence of FeS to J-phase, J-phase to X-phase, and X-phase to Li_2S (reactions 1, 2, and

4).

If the initial concentration of LiCl, x^o_{LiCl}, is increased, the two temperatures marked by the dashed lines will shift downward, bringing the regions of X-phase stability to lower temperatures, or making J-phase unstable at high temperatures.

The Thermodynamic, Open-Circuit Potential Behavior.—The rectangular regions in Figure 1, in which only reaction 3 or reaction 4 occurs, are three-phase regions. If we apply the Gibb's phase rule at constant temperature and pressure, we see that these two regions correspond to regions of constant potential during equilibrium discharge. The two triangular regions shown in Figure 1 are regions in which five phases are in equilibrium. These triangular regions are also regions of constant potential (at a given temperature), because the electrolyte is not involved in the overall reaction. The regions in which reactions 1, 2, or 5 occur alone are four-phase regions and have open-circuit potentials (relative to α-β LiAl) that vary with electrolyte composition.

Figure 2 gives the open-circuit potential behavior as a function of state-of-discharge for the same conditions as Figure 1: initially eutectic composition and one mole of electrolyte per mole of FeS. This type of plot can give insight into the potential-time profile for the reversible operation of a LiAl/FeS cell. The different lines refer to different percent utilizations during the discharge of a cell. The occurrence of reactions 1, 2, or 5 causes the electrolyte composition to vary with utilization. For example, the bands marked 0%, 1%, 5%, and 9% utilization reflect the dependence of the open-circuit potential on electrolyte composition for reaction 1. Similarly, the bands marked 12%, 23%, and 37% reflect the composition dependence of the potential of reaction 2, and the nearly horizontal bands are associated with reaction 5. The results
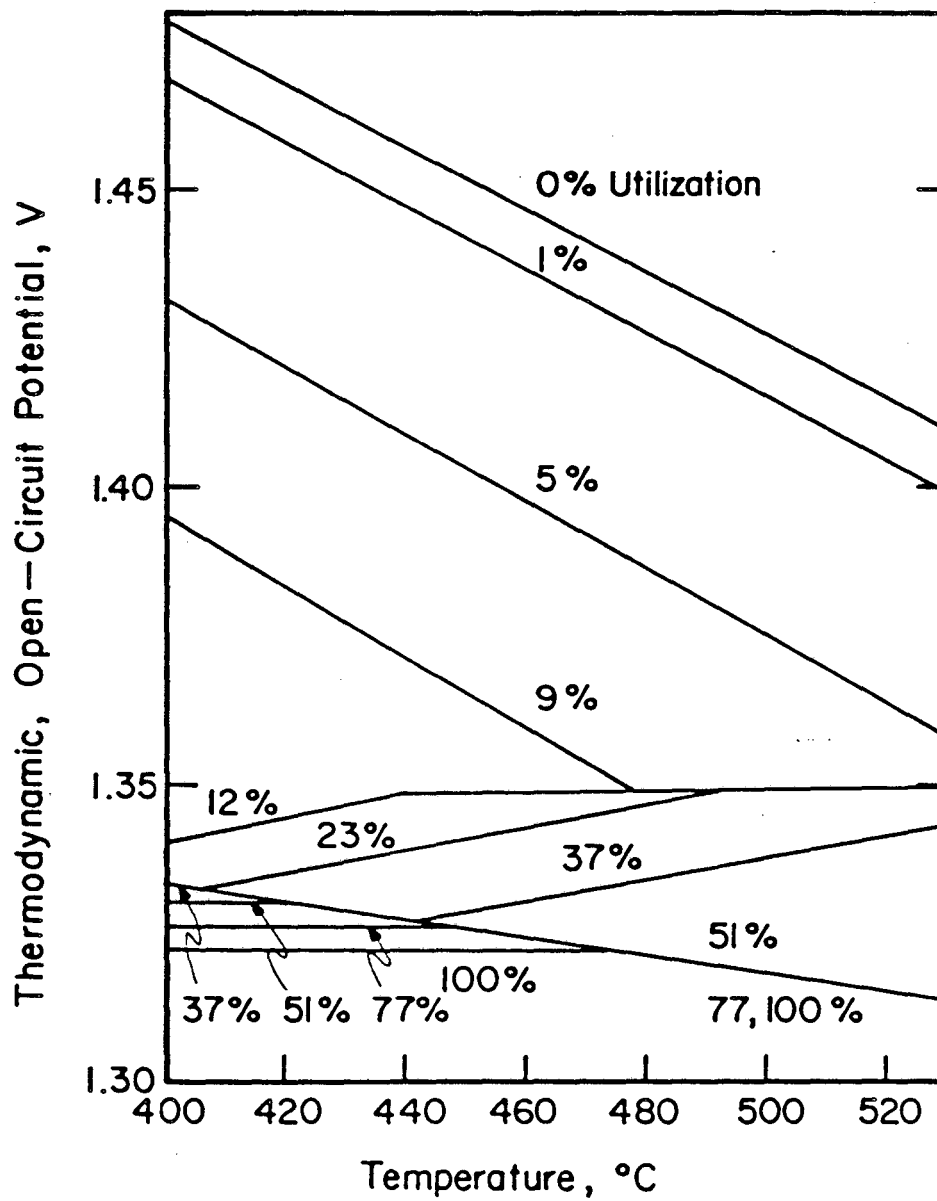
Figure 2. The open-circuit potential behavior as a function of temperature at different percent utilization for a cell with $x^0_{\text{LiCl}} = 0.58$ and $n^0_e = 1.0$.

shown in Figure 1 can be applied to the results in Figure 2 to determine the different reactions occurring for a given open-circuit potential as a function of utilization and temperature.

Figure 3 shows the open-circuit potential behavior for the same initial electrolyte composition as in Figure 2 (eutectic) and a larger electrolyte to FeS ratio ($n_e^o = 2.55$). These values of n_e^o and x_{LiCl}^o are the values used in the mathematical model that is discussed in the next section.

A larger value of n_e^o means that the cell in Figure 3 has more electrolyte than the cell in Figure 2. At a given state-of-discharge, the cell with $n_e^o = 2.55$ will be closer to the initial composition than the cell with $n_e^o = 1.0$. Comparing Figures 2 and 3, we can see that the bands representing the open-circuit potentials for reaction 1 (labeled 0%-9% utilization) shift toward the 0% utilization line with larger values of n_e^o. The intercepts, not the slopes, of the lines change. In the limit that n_e^o approaches infinity, the electrolyte composition will not change during discharge, and the series of bands shown for different utilization in the figures will converge to a single line. This is the situation discussed by Tomczuk et al.[9]

An increase in x_{LiCl}^o will shift the wedge shaped region of J-phase stability to lower temperatures. This can be seen by examining U_l for reactions 1, 2, and 5. For example, as can be seen from Equation 4 (for reaction 1), increasing x_{LiCl}^o will only slightly change the slope in this equation; the intercept will be changed much more. This effect is illustrated and discussed in Reference 9 for increasing x_{LiCl}^o from 0.58 to 0.67 with a value of n_e^o of infinity. The authors discuss how this increase is known to be sufficient to suppress the harmful effects of the J-phase on electrode performance in experimental
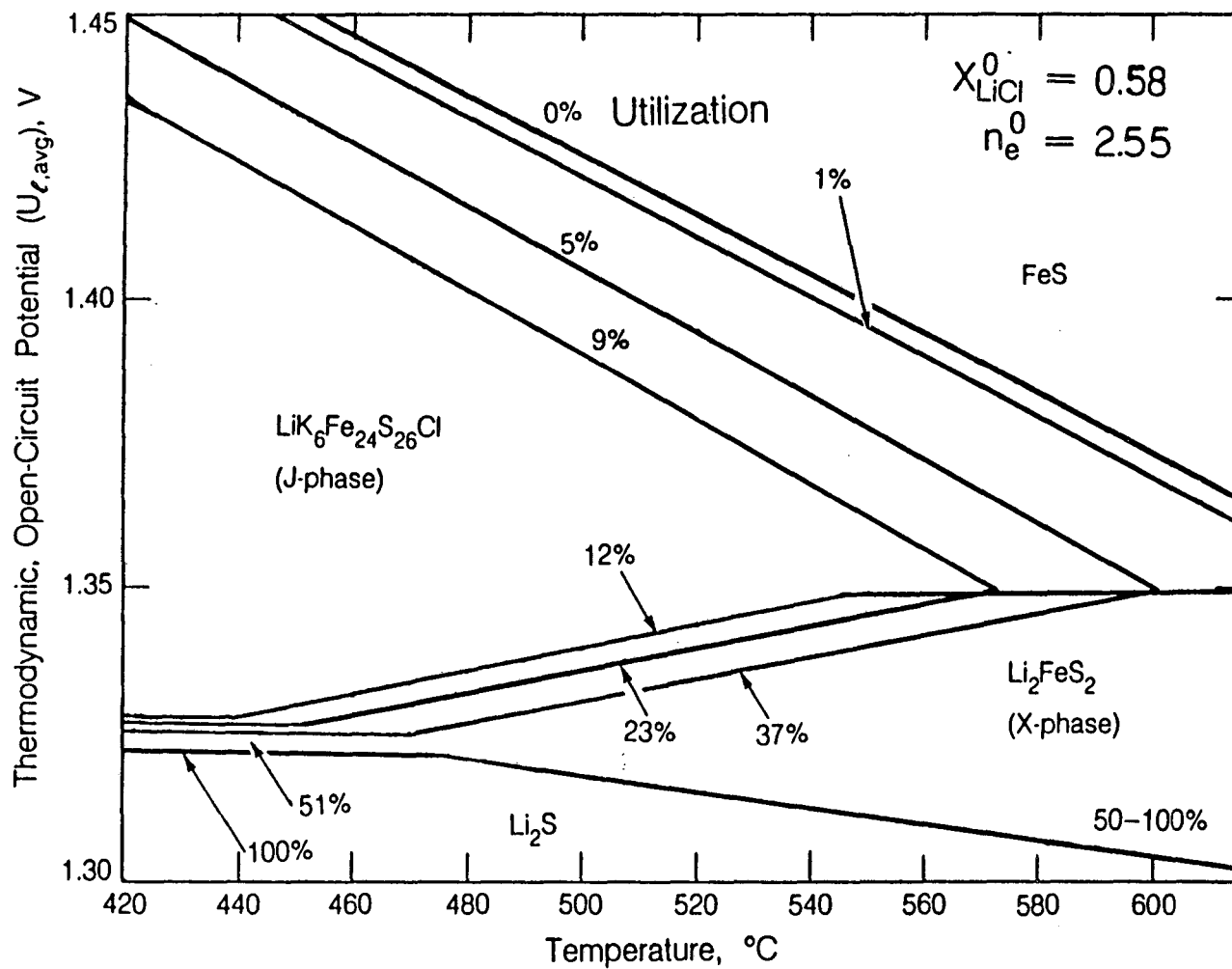
Figure 3. Calculated open-circuit potential behavior as a function of temperature at different percent utilizations for a cell with $x_{LiCl}^0 = 0.58$ and $n_e^0 = 2.55$.

cells.

LiAl/FeS Cell Model

A cross section of the cell sandwich is shown schematically in Figure 4. The model is one dimensional and consists of a porous negative electrode (shown on the left) and a porous positive electrode (shown on the right) with a reservoir and porous separator in between. The hatched area in the electrodes refers to the cell's active material (also called the matrix phase). The clear area refers to the molten LiCl-KCl electrolyte that fills the pores within the cell. The fundamental equations in the model are material balance equations for species in the electrolyte phase and matrix phase, an Ohm's law equation, a current balance equation, and electrochemical kinetic equations. The governing equations were originally developed by Pollard and Newman,[4,5] and we refer the reader to their work for the development of the equations and boundary conditions. These equations are cast into finite-difference form along with the appropriate boundary conditions and solved iteratively by the method of Newman.[14] The model calculates time-dependent behavior such as the cell voltage and temperature. The model also calculates position- and time-dependent behavior such as distributions of electrolyte composition, reaction rates, and porosity. A voltage balance gives the cell voltage, and an energy balance gives the cell temperature (assumed to be uniform throughout) and heat-generation rate. The kinetic equation for each reaction will give partial current densities, and individual material balances on the solid-phase species yield the volume fractions of solid phases.

MATRIX   ELECTROLYTE   RESERVOIR OF
                                  ELECTROLYTE

LiAl

FeS

CURRENT
COLLECTOR

NEGATIVE   SEPARATOR   POSITIVE
ELECTRODE   ELECTRODE

$$LiAl \rightarrow Li^+ + e^- + Al \qquad\qquad 2FeS + 2Li^+ + 2e^- \rightarrow Li_2 FeS_2 + Fe$$
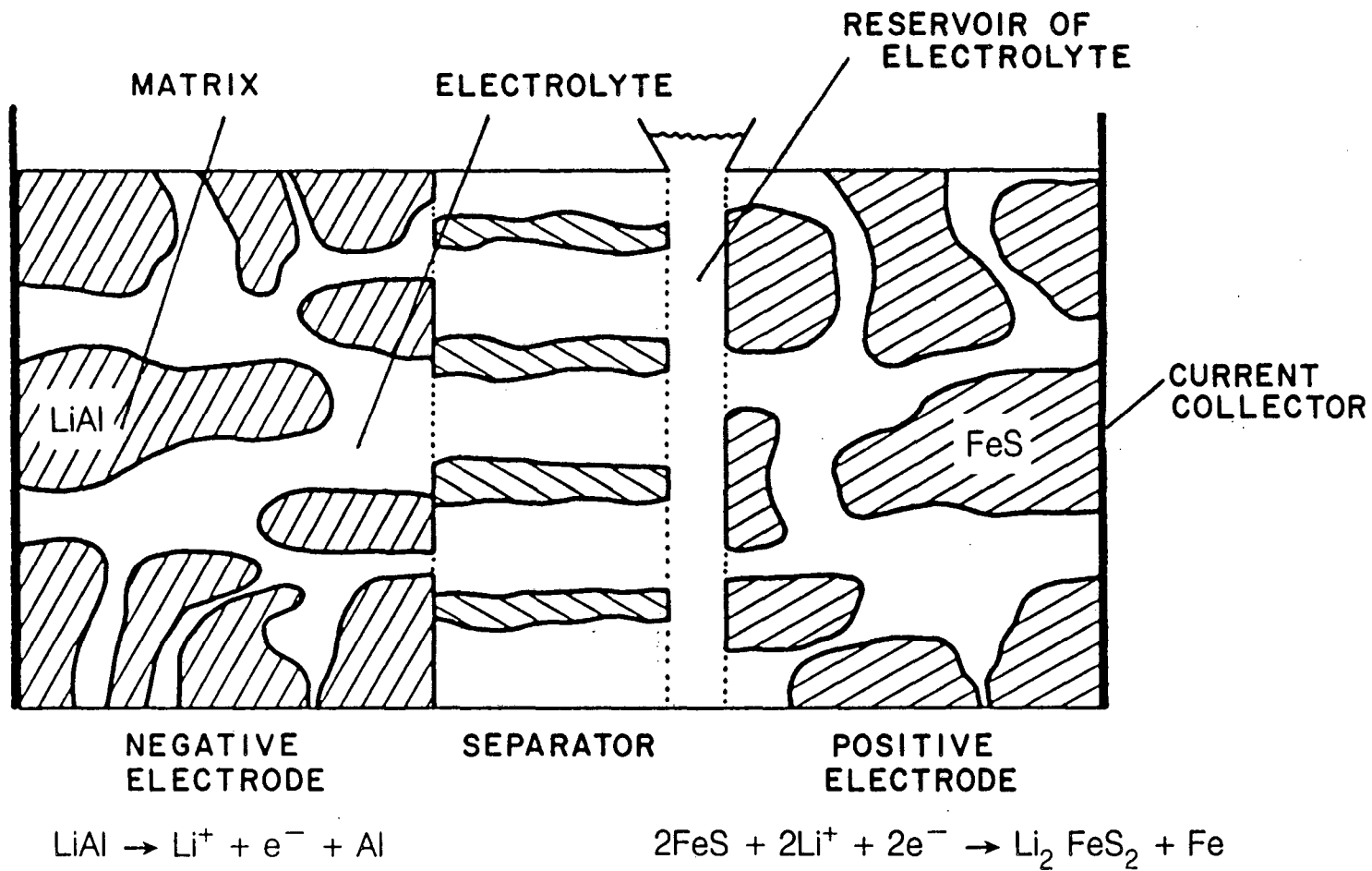
Figure 4. Schematic diagram of the LiAl/FeS cell.

XBL 849-8736

Modifications to Pollard and Newman's Original Model.[4,5]—In an effort to reduce capacity limitations by KCl precipitation, the kinetic equations were modified, and this is discussed in the next section. The energy balance has been modified to include heat effects due to simultaneous electrode reactions and electrolyte mixing. A general energy-balance equation is developed in Reference 15, and the results of applying it to the LiAl/FeS cell discharged with the X-phase and J-phase mechanisms are presented. In References 12 and 16, we discuss the modifications required for the simulation of a Li(Si)/FeS$_2$ cell and present results of this model.

Pollard and Newman observed that their model predicts the positive-electrode resistance to be about six times lower than experimental observations,[4,5] and that the resistance of the matrix phase is negligible ($\sigma_{matrix} \approx 10^4$ (Ω-cm)$^{-1}$). One possible explanation for this is the model calculation of the positive-electrode matrix conductivity. Measurements of the conductivity of X-phase have been published recently,[17] and it appears that the value used in the original model ($\sigma_X = 500$ (Ω-cm)$^{-1}$) is too large by a factor of 100. Changing the value of the conductivity of X-phase would only affect the resistance of the electrode when the second reaction of the X-phase mechanism occurs to an appreciable extent. The model does not predict the second reaction to occur to an appreciable extent before the cutoff voltage is reached. Therefore, changing σ_X to 6.3 (Ω-cm)$^{-1}$ could not explain the observed discrepancy.

The original model assumed parallel conduction paths in the electrode and combined the conductivities of the solid-phases in the electrode matrix by

$$\sigma_{matrix} = \sum_{i,solid} \sigma_i \, \epsilon_i^{1.5} \, . \tag{6}$$

Photomicrographs of coexisting phases of an FeS electrode indicate that the iron phase formed during discharge appears as discrete iron particles.[9] Iron is extremely conductive ($\sigma_{Fe} \approx 10^4$ (Ω-cm)$^{-1}$), and assuming a parallel conduction path for such a highly conductive material can give a very large matrix conductivity. For example, we can apply Maxwell's model[18] for solid phase conductivity to this system. With Maxwell's model, there is assumed to be a continuous phase and several discrete phases. We apply this model in the following manner. We assume that the discrete phases are Fe and voids. All other electrode phases are lumped together and called the continuous phase with the conductivity given by an average. For example, the conductivity of the continuous phase of the FeS electrode discharged through the X-phase mechanism would be written as

$$\sigma_{continuous} = \frac{\epsilon_X \, \sigma_X + \epsilon_{Li_2S} \, \sigma_{Li_2S} + \epsilon_{FeS} \, \sigma_{FeS}}{\epsilon_X + \epsilon_{Li_2S} + \epsilon_{FeS}} \, . \tag{7}$$

We can then apply Maxwell's equation in this manner to give the matrix conductivity,

$$\frac{\sigma_{matrix}/\sigma_{continuous} - 1}{2 \, \sigma_{matrix}/\sigma_{continuous} + 1} = \left(\frac{\sigma_{Fe}/\sigma_{continuous} - 1}{2 \, \sigma_{Fe}/\sigma_{continuous} + 1} \right) \epsilon_{Fe} - \epsilon \, . \tag{8}$$

We shall compare the effective conductivities of the positive electrode calculated with Equations 6 and 8. After exhaustion of FeS, for the base-case operating conditions in Table 3, $\epsilon_X = 0.55447$, $\epsilon_{Fe} = 0.08522$, and $\epsilon = 0.36030$. We calculate $\sigma_{matrix} = 2050$ (Ω-cm)$^{-1}$ and 2.62 (Ω-cm)$^{-1}$ from Equations 6 and 8, respectively. If we assume, as an

extreme case, that all the current is going to the second reaction, then the potential differences across the matrix phase are 3×10^{-3} mV and 3 mV for Equations 6 and 8, respectively. This does not explain, however, the ≈ 40 mV discrepancy that is discussed by Pollard and Newman.[4,5] Equation 8 is an improvement in the estimation of the matrix conductivity over Equation 6; however, the discrepancy between model and experimental electrode resistances is not fully explained and requires further investigation.

The J-phase mechanism (reactions 1 and 3) is written as

$$26\text{FeS} + \text{Li}^+ + \text{Cl}^- + 6\text{e}^- \longrightarrow \text{J} + 2\text{Fe}$$

and

$$\text{J} + 51\text{Li}^+ + 46\text{e}^- \longrightarrow 26\text{Li}_2\text{S} + 24\text{Fe} + 6\text{K}^+ + \text{Cl}^- \ .$$
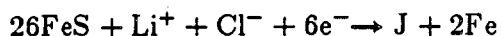
The open-circuit potentials are given by Equations 2 and 3 with the coefficients for reactions 1 and 3 in Table 2. The open-circuit potentials of the reactions in the J-phase mechanism, relative to the LiAl electrode, are dependent on electrolyte composition and temperature. In contrast, the open-circuit potentials of the reactions in the X-phase mechanism are only functions of temperature. Consequently, the surface overpotentials, $\eta_{s_l} = \eta - U_{l,o}$, for the above reactions have an additional dependence on the electrolyte composition variable: x_{LiCl}.

The voltage gap between the potential plateaus for the reactions of the X-phase mechanism does not vary with temperature as much as the potential gap for the J-phase mechanism (see Figure 3). Consequently, for the X-phase mechanism we assume that

the gap is constant at 0.0326 V.[4,5] Since the cell temperature will typically rise only about 10°C during discharge at the base-case operating conditions (see Figure 1 of Reference 15), this is not a bad approximation. For the J-phase mechanism, the temperature rise may be 30 to 40°C. The variation of this potential gap with temperature must be included in the model.

Operating Parameters.—Many of the operating parameters are the same parameters that were used in Pollard and Newman's original work.[4,5] For example, the negative electrode operating variables are unchanged, and we refer the reader to Pollard and Newman's work for these values (Figure 9 of Reference 5). The appendix of Pollard and Newman's work[4,5] gives formulas for the composition and temperature dependence of conductivity, transference number, molar volume, and diffusion coefficient of the electrolyte and for the temperature dependence of the saturation concentrations of LiCl and KCl. The original, literature data in Table 2 for reactions 1 and 5 were used for the equilibrium potentials because we had not yet worked out the thermodynamically consistent values. We used the same values as Pollard for the exchange current densities. The molar volume of J-phase (669.69 cm^3/mole) was taken from Reference 17. The conductivity of J-phase was assumed to be that of X-phase. Table 3 provides the operating parameters for a base case corresponding to the conditions of Figure 9 in Reference 5. Deviations from these values are noted in the figure captions.

Table 3. Base-Case Input Data.

Quantity	Value	Quantity	Value
x^o_{LiCl}	0.58(eutectic)	i	0.0416 A/cm^2
T_o	743.15 K	T_A	298.15 K
Q_+	4630 C/cm^3	ϵ^o_{FeS}	0.445
Q_-	2800 C/cm^3	ϵ^o_+	0.555
L_+	0.18 cm	ϵ^o_-	0.39
L_-	0.32 cm	ϵ^o_s	0.75
L_s	0.16 cm	m	∞

Results and Discussion

As we mentioned earlier, the presence of J-phase in experimental cells is believed to be undesirable because the reactions involving this phase are slow, which causes difficulties in cell charging.[3] Despite the undesirability of J-phase, it is important to understand the effects that it has on cell behavior. This understanding helps us to define which factors are likely to improve the performance of the FeS electrode.

Electrolyte Composition Changes During Discharge.—During the discharge of a LiAl/FeS cell, the effects of diffusion, migration, convection, and nonuniform reaction distribution result in a spatial variation of electrolyte throughout the cell sandwich. The contribution of convection arises primarily from the squeezing of the electrolyte as the porosity changes. Figure 5 shows model calculations of composition profiles across a
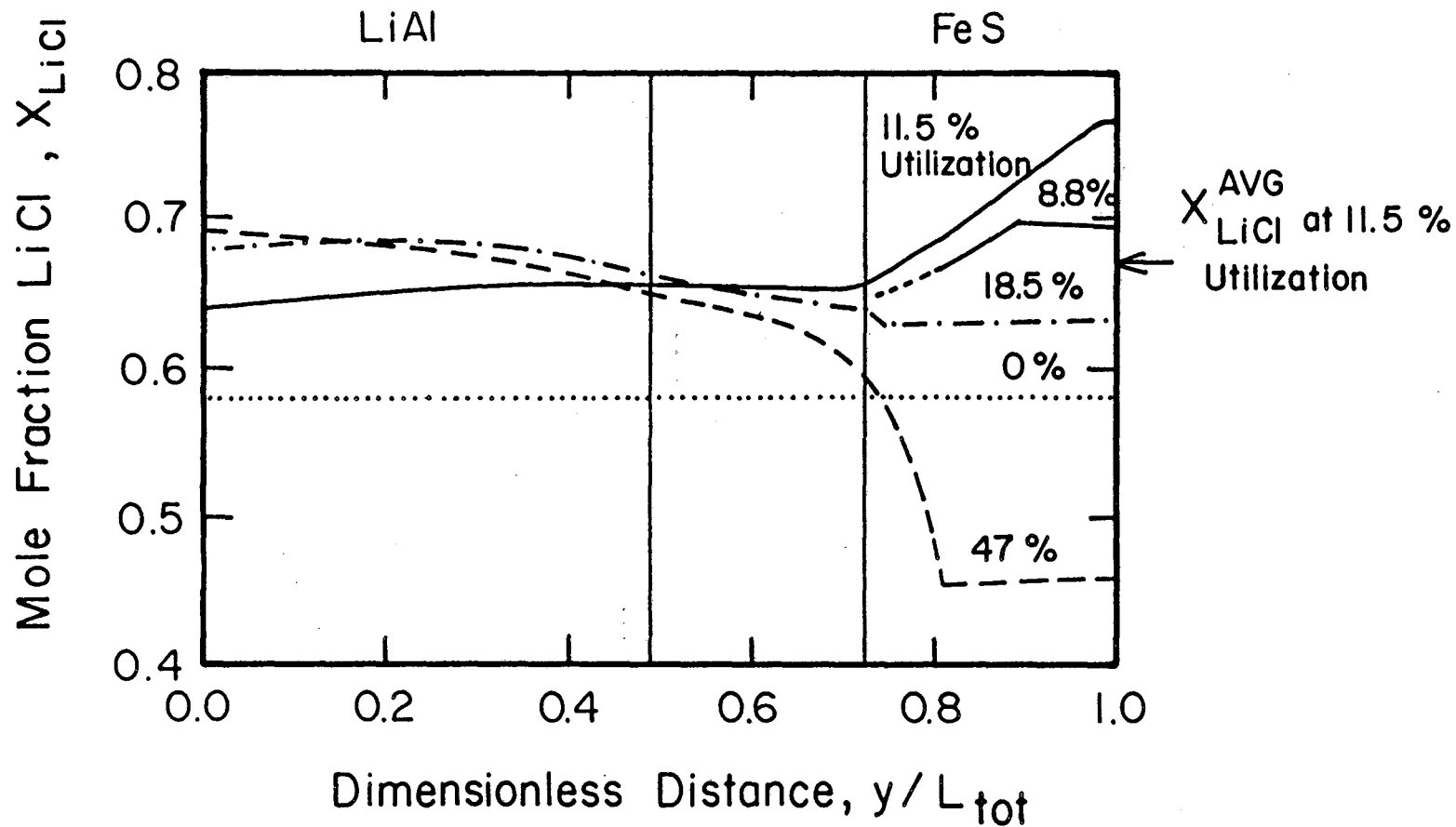
Figure 5. Position dependence of the mole fraction of LiCl at different states of discharge for the J-phase mechanism. Simulation parameters are for the base case (Tables 2 and 3).

cell, with J-phase as the intermediate in the positive electrode, at several states-of-discharge. The mathematical model predicts that the reactions do not occur simultaneously. That is, FeS is completely exhausted by the first reaction (at 11.5% utilization) before the second reaction occurs. Prior to the onset of the second reaction, the mole fraction profiles exhibit a maximum at the position of the first reaction front. In Figure 5, the maximum is at $y/L_{tot} = 0.88$ and 1.00 for 8% and 11.5% utilization, respectively. The composition profiles given by Pollard and Newman for the X-phase mechanism exhibit a minimum at the position of the first reaction front in the positive electrode (Figure 2 of Reference 5). At 11.5% utilization, x_{LiCl} is large enough at the back of the electrode ($y/L_{tot} = 1.00$) that the second reaction begins there. Soon after 12% utilization, x_{LiCl} has decreased enough that the position of the second reaction front moves to the electrode-reservoir interface. In Figure 5 the position of the second reaction front is at the minimum in the composition profile for 18% and for 47% utilization. At 47% utilization the cutoff voltage is reached. The capacity-limiting mechanism for the cell is the clogging of pores by KCl precipitation in the positive electrode. It should be mentioned that the cell temperature increases 35 degrees during discharge (see Figure 1 of Reference 15). For the same operating conditions, simulation of discharge behavior with the X-phase mechanism results in a much lower maximum utilization ($< 40\%$). The switching of the position of the second reaction front from the back to the front of the electrode with the J-phase mechanism allows for more uniform utilization of active material and is one of the reasons for the longer cell discharge time. Even at isothermal operating conditions (all other conditions the same) the cell with the J-phase mechanism yields 45% utilization.

Cell Voltage Behavior.—Figure 6 ($m = \infty$, $\epsilon_+^o = 0.555$) gives the cell voltage as a function of utilization for the base-case operating conditions. In the region from 0% to 11.5% utilization, the open-circuit potential decreases because x_{LiCl} increases and the cell temperature increases. The decline of the open-circuit potential is partially responsible for the observed voltage drop in this region.

As explained earlier, we expect the J-phase mechanism to be observed in experimental cells at relatively low temperatures. For cells with a large excess of electrolyte, we would expect the J-phase mechanism to occur for temperatures less than 475.8°C. For more electrolyte-starved cells, the J-phase mechanism would occur for temperatures less than 440°C and 377°C for $n_e^o = 2.55$ and 1.0, respectively (see Figures 1, 2, and 3). Figure 7 shows the voltage behavior of an experimental cell at a low enough temperature that a pure J-phase discharge mechanism should occur.[9,12] The charge and discharge voltage behaviors are asymmetric in experimental cells that operate with the J-phase mechanism and are more symmetric with the X-phase mechanism: the cells operating with the J-phase mechanism are difficult to charge, and a maximum utilization of 73% is observed experimentally. At these operating temperatures and the base-case operating conditions, our model would predict the cutoff voltage to be reached before 47% utilization. The capacity limitations, which are caused in the model by KCl precipitation, are discussed in the next section.

Although the model is not capable of simulating the other possible reactions along with the J-phase mechanism, it is interesting to examine whether the occurrence of these other reactions becomes possible. The model predicts that the overpotential within the positive electrode is not great enough for the conversion of FeS to X-phase to occur.
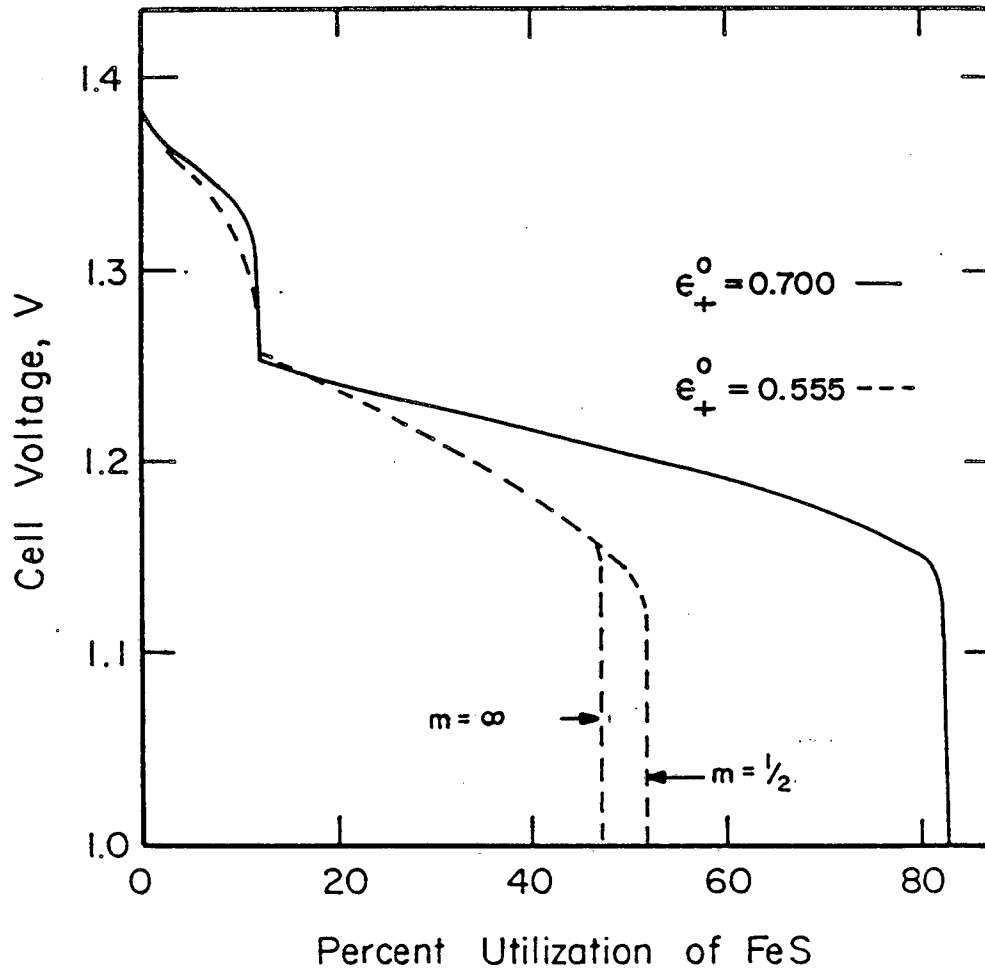
Figure 6. Cell voltage as a function of positive electrode utilization for the J-phase

mechanism for two values of m and ϵ_+^o. Simulation parameters are for the base case

except m and ϵ_+^o.
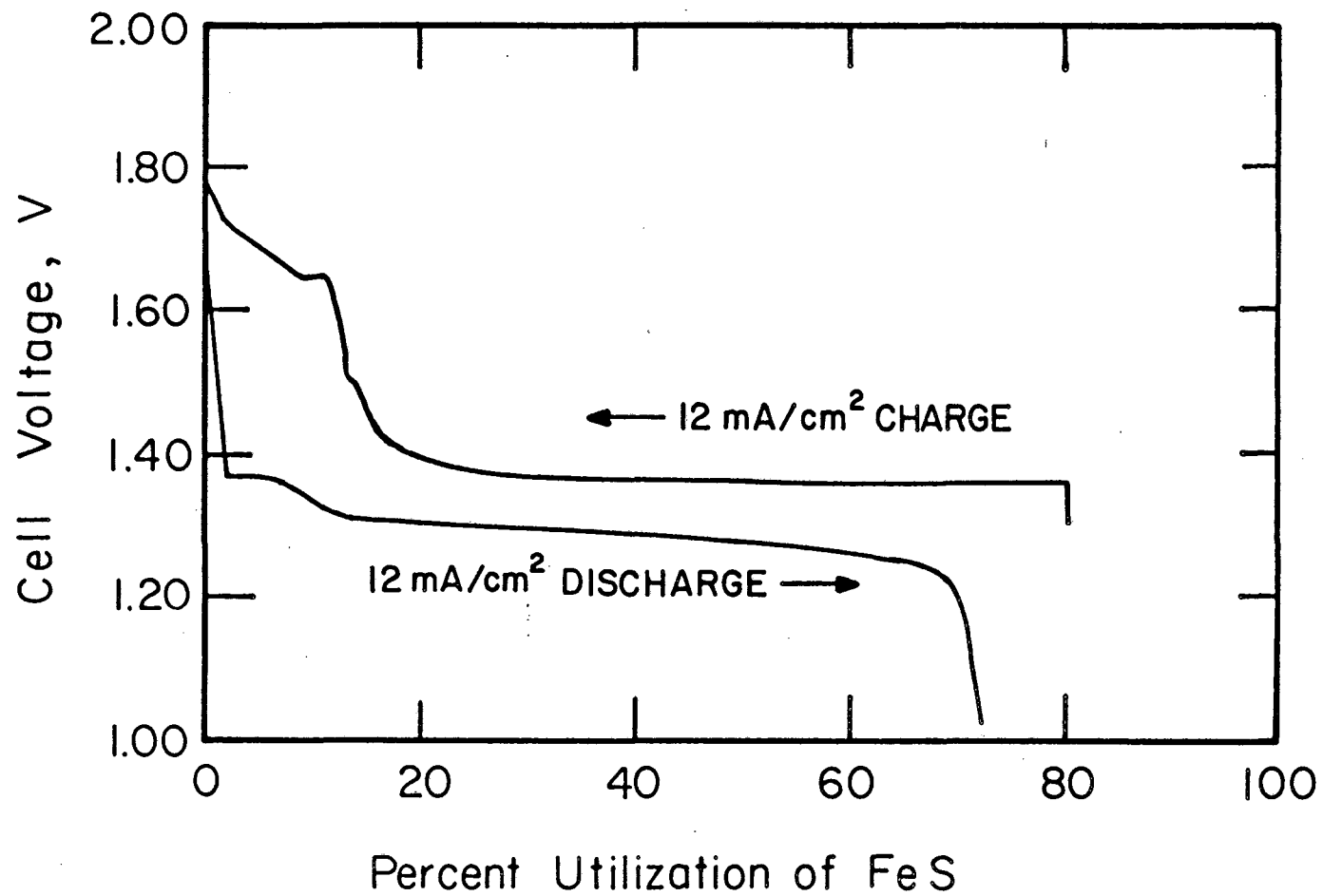
Figure 7. Experimental cell voltage as a function of positive electrode utilization at 443°C using electrolyte of eutectic composition.[9]

This is in harmony with experimental observations at these operating conditions. In the model, we assume that J-phase is directly converted to Li_2S and Fe in a single reaction, and the onset of this reaction is predicted to occur at 11.5% utilization. The J-phase to X-phase transition would occur at this utilization if the model had the capability of simulating this reaction. Then, the reactions of J-phase and X-phase being converted to Li_2S and Fe would occur as the overpotentials within the electrode became greater. A model including the five, possible, positive-electrode reactions may predict a larger maximum utilization than the models with only the J-phase mechanism or the X-phase mechanism. The incorporation of more reactions should allow more uniform utilization of active material. This will tend to delay the precipitation of KCl in the positive electrode and increase the prediction of the maximum utilization of the cell.

The Effects of KCl Precipitation on Positive-Electrode Utilization.—The principal capacity-limiting mechanism predicted by the mathematical models is the plugging of the porous positive electrode with KCl precipitate. This causes the cell voltage to drop sharply to the cutoff point at relatively low utilization (< 60%). In contrast, experimental cells operating under similar conditions exhibit much greater capacities (> 80% utilization) and smoother voltage declines to the cutoff point. Crystals of KCl have been observed in experimental cells discharged at approximately 430°C.[3] It appears, however, that the models either severely overestimate the effects of precipitation or predict the precipitation prematurely. There are many possible explanations for the discrepancy between theoretical and experimental results, and Pollard and Newman[4,5] examine them in their work. The authors conclude that mixing by natural convection, supersaturation, and local heat effects are unlikely explanations for the discrepancy.

Other possible reasons are electrode expansion, precipitate morphology, which can affect the reaction distribution, modification of the solubility limit by impurities, and possible conductivity of the KCl precipitate. The last two reasons will be addressed in the following discussion. The first two reasons will be discussed in a later section.

The simulated cell voltage behavior for a cell with the solubility limit modified so that precipitation does not occur at all during discharge is more representative of the behavior that is observed in experimental cells than model results with precipitation.

One other point to consider is relaxing the assumption that the KCl precipitate is completely insulating. If the precipitate were about as conductive as the electrolyte, we would expect the cell voltage behavior to be similar to the results obtained without consideration of KCl precipitation. However, the transference number of lithium should be zero in the precipitate.

The precipitation of LiCl or KCl salts may affect the rates of the electrochemical reactions occurring within the pores of the electrode. This is accounted for by assuming that the interfacial active area per unit volume of electrode a is related to the amount of precipitate by the expression,

$$a = a_o \left[1 - \left(\frac{\epsilon_p}{\epsilon + \epsilon_p} \right)^m \right],$$

where m is an adjustable parameter. Notice that a is decreased with an increase in the amount of precipitate. The morphology of the precipitate is reflected by the value of m. For instance, if m is zero, then a passivating, film-type precipitate is implied, and the electrode reactions cannot occur in the region of precipitation. The reaction rates are

not affected by precipitation if m is very large. This may describe the case of a salt that forms a very thin, needle-like precipitate. We would expect more utilization of active material as the value of m is decreased from infinity. For example, for the X-phase mechanism, when m is decreased from infinity to 1.0 to 0.5, the maximum utilization increases from 52.1 to 53.6% to 55.4%. For very small values of m, however, the maximum utilization of the cell decreases; in the limit of $m = 0$, utilization of active material halts in the region of precipitation. We have not investigated results with m smaller than 1/3.

The high temperatures and high values of $i_{o,l}$ for this system cause rapid, localized reactions to occur within the electrode. As a result, a highly nonuniform reaction distribution results. We have compared the transfer current distributions for the first reaction of the X-phase mechanism for two values of m. A reaction front gradually moves through the electrode as active material is consumed. KCl will precipitate in the region of highest transfer current. If the precipitate is allowed to inhibit the electrode reaction, then we would expect the reaction front to be more spread out within the electrode. In other words, by decreasing m, a reaction will be more uniformly distributed. The reaction front is thicker for the case of $m = 0.5$ than for $m = \infty$. The precipitated regions correspond approximately to the thickness of the fronts. The thicker reaction front has precipitate distributed more uniformly, and the porosity is larger, than in the case with the thin reaction front. For the case of $m = \infty$, the transfer current is actually slightly positive in back of the reaction front (about 0.14 cm). This phenomenon of bipolarity is not observed at this utilization for the case of $m = 0.5$.

Prior to the onset of precipitation at 26.0% utilization, the reaction distributions are identical. The same capacity-limiting mechanism usually occurs for the smaller value of m; however, a greater depth of discharge is achieved (55.4% for $m = 0.5$ versus 52.1% for $m = \infty$) before the cutoff voltage is reached. The more uniform reaction distribution is responsible for the longer discharge-time of this cell.

Figure 6 shows the cell voltage behavior for the J-phase mechanism and two values of m. When m is decreased from infinity to 0.5, the maximum utilization increases from 47% to 51%. The point where the two curves diverge corresponds to the onset of precipitation. It should be noted that there is a large temperature excursion during discharge at these operating conditions. Figure 1 of Reference 15 gives the temperature profile for the case of $m = \infty$. The temperature profile for the case of $m = 0.5$ is identical to the case of $m = \infty$ up to 47% utilization. With an initial porosity of 0.60, the maximum utilization increases from 58.8% to 60.0% when m is decreased from infinity to 0.5.

The results of modeling both the X-phase and J-phase mechanisms show that increasing the initial porosity of the FeS electrode gives an increase in the cell utilization. One reason for this is that the increased pore volume allows more precipitation before the pores are blocked and the cell voltage drops to the cutoff point. The electrolyte concentration profile and reaction distributions throughout the electrode are also affected. In practice, highly porous electrodes with good mechanical stability are difficult to construct. Electrode expansion is observed experimentally and is not accounted for in the models. Later, we will relate the results of varying the initial porosity to the expansion phenomenon.

The model results for the X-phase mechanism show the utilization for the initial porosity of the FeS electrode of 0.555, 0.655, and 0.755 yield utilizations of 32%, 42%, and 75%, respectively.[12] All three electrode have the same capacity (833.3 C/cm^2), so that an increased porosity corresponds to a thicker electrode. For a given utilization, the case with the largest ϵ_+^o gives the highest cell voltage. This is primarily an ohmic-resistance effect in the electrolyte phase (which is more resistant to current flow than the matrix phase); the current in the pores must follow a more tortuous path for the case with $\epsilon_+^o = 0.555$ than for the case with $\epsilon_+^o = 0.755$.

The porosity of the electrode also affects the reaction distribution. At 10% utilization, the transfer current at the position of the reaction front is four times larger for the case of $\epsilon_+^o = 0.655$ than for the case of $\epsilon_+^o = 0.755$. This lowering of the transfer current also works to delay precipitation.

Figure 6 shows the cell voltage versus utilization for the J-phase mechanism and two values of ϵ_+^o ($m = \infty$). We see that an increase in the initial porosity of the positive electrode from 0.555 to 0.700 increases the cell utilization from 47% to 83%. The capacity-limiting mechanism in both cases is the blockage of pores by KCl precipitate in the positive electrode. The precipitation of KCl occurs at 45% and 75% utilization for the case of $\epsilon_+^o = 0.555$ and 0.700, respectively. Unlike the results for the X-phase mechanism, the cell reaches the cut-off voltage just after the onset of precipitation. Two considerations lead to an explanation as to why the precipitation has such a drastic effect with the J-phase mechanism relative to the X-phase mechanism results. Unlike the X-phase mechanism, the first reaction of the J-phase mechanism is more exothermic than the second. Furthermore, KCl is a product of the second reaction.

We shall now investigate the results of varying ϵ_+^o, which can help aid in the understanding of the effect that positive-electrode expansion has on experimental cells. Our mathematical model does not account for electrode swelling during discharge. The model assumes that as the solid phase expands during discharge, the positive electrode becomes less porous. Similarly, the negative electrode's active material shrinks during discharge, and the electrode becomes more porous. The model predictions of lower utilization than is observed experimentally can, in part, be explained by expansion of the positive electrode. Pollard and Newman[4,5] use the value of $\epsilon_+^o = 0.555$ for their model in their comparison to experimental cell discharge behavior. This initial porosity corresponds to a capacity density of 1.286 A-hr/cm^3 ($\epsilon_{FeS}^o = 0.445$) and can be compared to the value of 1.4 A-hr/cm^3 ($\epsilon_{FeS}^o = 0.484$, $\epsilon_+^o = 0.516$) that is used in the construction of the experimental cells.[1] Pollard and Newman used the slightly larger initial porosity in an attempt to account for the swelling of the positive electrode. More recently, experimental measurements of the positive electrode expansion have been made; it appears that the expansion is greater than originally assumed.

In experimental cells, the phase changes that occur during discharge-charge cycles subject the active-material solids to forces that tend to cause an electrode to expand and disperse particles out of the electrode boundary. This extrusion of material may cause bridging of the electrodes and short circuit. Short circuit has been a primary mode of failure in experimental cells, but it can be circumvented by improved mechanical construction of the electrodes.[1] Experimental cells are usually constrained at the faces and edges in an attempt to prevent expansion. Cells that are examined after discharge-charge cycles usually exhibit expansion of both the positive and negative electrodes,

relative to the size of the as-fabricated electrodes.[1] Elliott and Cooper[19] studied the change in thickness of a cell sandwich (assembled in the fully charged state) over eight discharge-charge cycles. The cell exhibited a large initial, permanent expansion during the first three discharge-charge cycles, which is ascribed to expansion of the positive electrode. From the third to the eighth cycle, a cyclic, expansion-contraction, discharge-charge pattern was observed. It seems reasonable to conclude from these results that positive electrodes in experimental cells expand most in the first few cycles and maintain a steady average thickness for the remainder of cycle life. This may explain why the maximum utilization during discharge is usually low for the first cycle, increases during the break-in cycles, and is relatively constant thereafter.[1] We can define the percent expansion of the positive electrode during n cycles as the percent increase in thickness over the original thickness:

$$\% \text{ Expansion } = 100 \, \frac{L_+^n - L_+^1}{L_+^1} \, .$$

L_+^n refers to the total electrode thickness in a cell like the one that is mathematically modeled or the half thickness of the electrode in a bicell (two outer negative electrodes with a positive electrode in between). We can define the percent expansion in terms of porosity in the charged state ϵ_+^o from the relationships: $\epsilon_{FeS}^{o,1} \, L_+^{o,1} = \epsilon_{FeS}^{o,n} \, L_+^{o,n}$ (the theoretical capacity remains constant) and $1 - \epsilon_{FeS}^o = \epsilon_+^o$. The superscript o implies that the porosity is that of an electrode in the fully charged state.

Quantitative measurements of positive-electrode expansion at the end of cycle life are available.[1] Positive electrodes that were assembled with 0.155 cm half-thicknesses and $\epsilon_+^{o,1}$=0.53 were observed to expand 16, 23, and 29% after 804, 1031, and 559 cycles,

respectively. We calculate: $\epsilon_+^{o,804} = 0.60$, $\epsilon_+^{o,1031} = 0.62$, and $\epsilon_+^{o,559} = 0.64$. With this information, we can speculate that well-cycled cells really operate with charged-state porosities between 60 and 65%, even though the as-fabricated porosity is only 53%. Experimental data of the positive electrode-expansion within a cycle are also available and will be discussed later.

Figure 8 gives model predictions for the maximum utilization of a cell discharged through the J-phase, positive-electrode mechanism versus the initial porosity of the positive electrode. All the simulations have the same capacity, heat-transfer characteristics, and capacity-limiting mechanism (KCl precipitation). At first we shall concentrate on the 0% expansion line. We have assumed that in this range there is a linear relationship between the maximum utilization and ϵ_+^o as shown by the solid dots on the figure. There are data available for positive electrodes in bicells with half-thicknesses of 0.155 cm. These cells were fabricated with an initial porosity of $\epsilon_+^{o,1} = 0.53$, which corresponds to a capacity density of 1.358 A-hr/cm^3 (4889 C/cm^3) and capacity per unit area of 757.9 C/cm^2. As a first example, we can use Figure 8 to estimate 41.6% for the maximum utilization of this cell.

Now let us assume that the cell was observed in the fully charged state after 130 cycles, and the positive electrode had expanded 14% from the as-fabricated electrode. That is, the electrode half thickness was measured as 0.1767 cm, and the capacity density decreased to 1.191 A-hr/cm^3 (4289 C/cm^3). Of course, the capacity per unit area remained constant at 757.9 C/cm^2. The porosity $\epsilon_+^{o,131} = 0.5877$ allows us to predict the cell to achieve 55% utilization on the 131st discharge. In the preceding development, we have tried to account for the permanent expansion of the positive electrode.
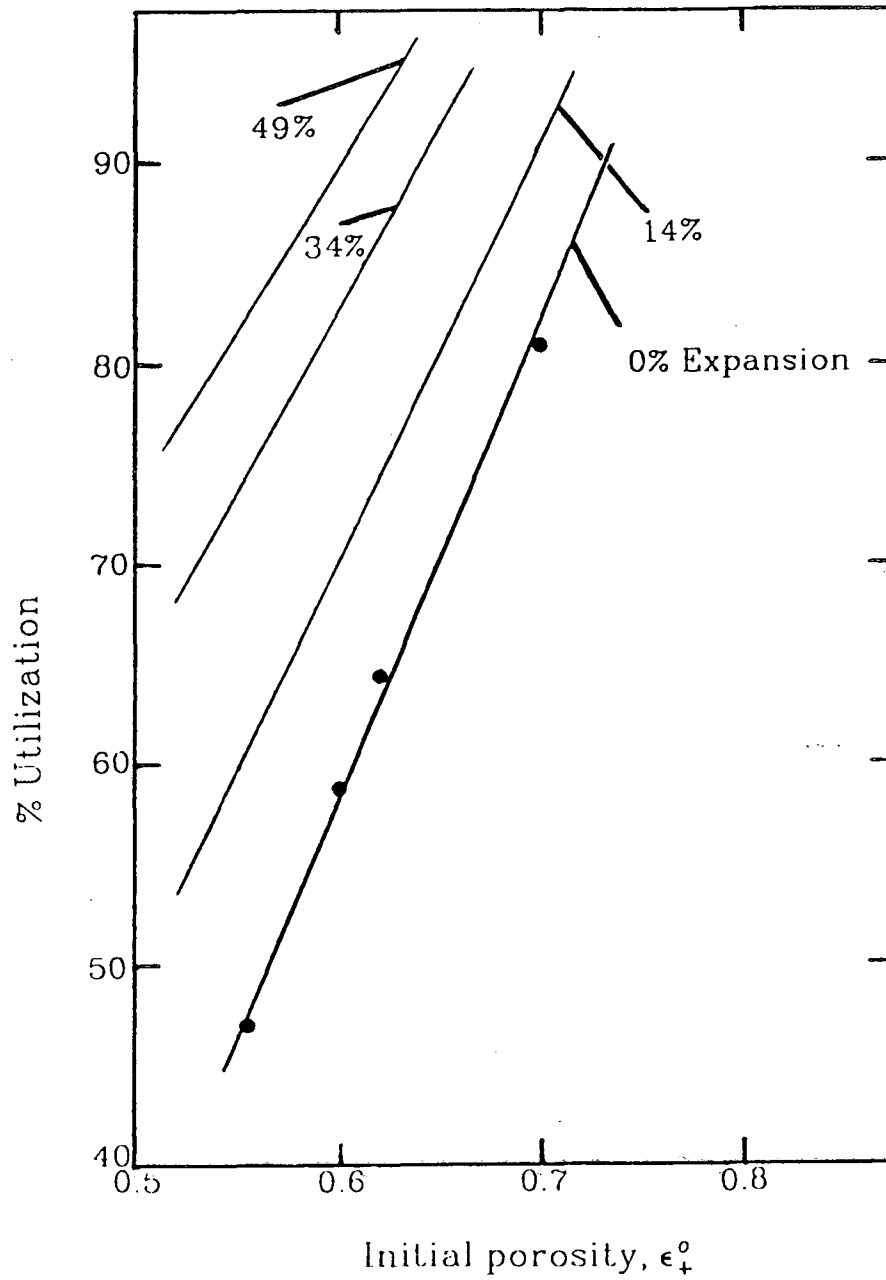
Figure 8. Maximum positive electrode utilization as a function of ϵ_+^o. The points are simulation results.

In the next few paragraphs we shall try to account for the expansion of the positive electrode that is cyclic, not permanent.

Figure 9 presents graphically the average percent expansion during discharge and charge of a series of experimental cells.[1] All of the cells are well-cycled and exhibit a steady expansion-contraction pattern during discharge-charge cycles. The figure shows that the average positive electrode exhibits a permanent expansion of 14% (in the fully charged state) over the as-fabricated electrode (also in the fully charged state). The average cell has expanded 49% at the end of discharge.

The information in Figure 9 can be used to interpret the information in Figure 8 more liberally. One may predict the maximum utilization of a cell accounting for expansion of the positive electrode during a discharge. In the previous discussion, we saw that, relative to the as-fabricated electrode, a well-cycled electrode is 14% expanded in the fully charged state and 49% expanded in the discharged state. We might expect that the simulation of well-cycled LiAl/FeS cells should allow for expansion somewhere in the range of 14 to 49%. If 14% expansion is assumed, Figure 8 yields the underestimated prediction of 55% utilization, and if 49% expansion is assumed we would expect an overestimated prediction of the maximum utilization. If we assume 49% expansion from the as-fabricated electrode, the electrode half thickness would be 0.2310 cm, and the capacity density would have decreased to 0.912 A-hr/cm^3 (3281 C/cm^3). Of course, the capacity per unit area remains constant at 757.9 C/cm^2. The porosity $\epsilon_+^{o,131} = 0.6846$ allows us to predict the cell to achieve 78.3% utilization on the 131st discharge.

A compromise value of expansion, between 14 and 49%, would yield the predicted maximum utilization between 55% and 78.3%. We may speculate that the compromise
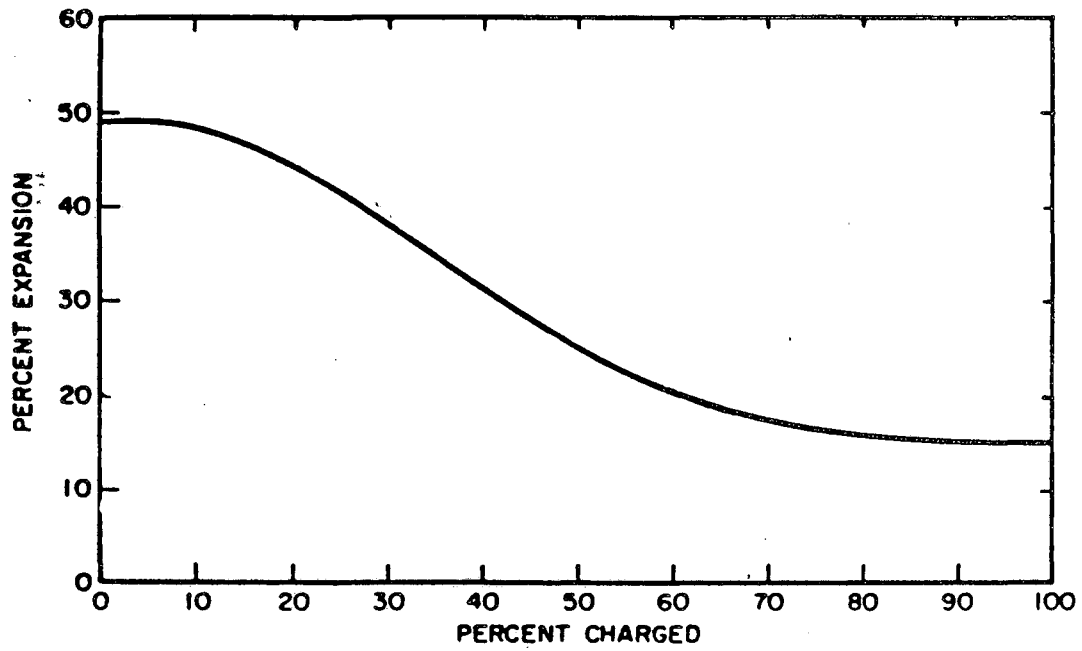
Figure 9. Average positive-electrode expansion of a series of experimental cells as a function of state-of-charge.[1]

expansion value should lie closer to the value of 49% than 14% because KCl causes limitations of utilization in the latter stage of discharge. The choice of a compromise of 34% expansion corresponds to a positive electrode half thickness of 0.2077 cm and a capacity density of 1.014 A-hr/cm^3 (3649 C/cm^3). For this example, we can calculate $\epsilon_+^{o,n} = 0.6493$, and the value of 69.8% utilization of FeS is predicted. The lines for various values of percent expansion in Figure 8 have been added as a convenience.

As mentioned earlier, experimental cells typically achieve 80% utilization of FeS during discharge. Our mathematical model results (Figure 8) give 80% utilization of FeS with $\epsilon_+^{o,n} = 0.69$, or an electrode that has expanded 51.6% from the as-fabricated electrode. Since this degree of expansion is not in the range of 15 to 49%, we should conclude that we have not fully accounted for the discrepancy in maximum utilization between experimental and theoretical results with expansion. The precipitation parameter m may account for the remaining discrepancy. Recall that the precipitation parameter $m = \infty$ was used in plotting Figure 8. The results of Figure 6 show that for the case of $m = \frac{1}{2}$ the model gives a larger maximum utilization of the positive electrode than the case with $m = \infty$. We can conclude that the simulation of well-cycled LiAl/FeS cells should allow for expansion by using values of ϵ_+^o between 0.59 and 0.68 and a compromise value of 0.65 is recommended.

Future modeling efforts should account for the variations in positive- and negative-electrode thicknesses during discharge. Experimental data of the electrode thickness as a function of time[1] could be incorporated into the model.

Conclusions

We have discussed the thermodynamic, open-circuit potential behavior of the LiAl/FeS cell as a function of state-of-discharge and temperature. This thermodynamic information is derived from the primary data (activity coefficients as a function of electrolyte composition and open-circuit potential data at a single composition) available in the literature. We have used the primary data to formulate a consistent set of thermodynamic data for the FeS electrode reactions. Calculations of the open-circuit potential compared to results of experimental cells show reasonable agreement. The composition dependence of the open-circuit potential is completely determined if the activity-coefficient behavior of the electrolyte species is known. It is important that primary data are available for thermodynamic analysis of this system.

The simulated cell voltage behavior with the J-phase mechanism shows reasonable agreement with the behavior of an experimental cell at conditions in which we would expect the positive electrode to discharge through the J-phase mechanism. The main capacity-limiting mechanism predicted by the mathematical models (for both the X-phase and J-phase mechanisms) is the clogging of pores by KCl precipitation in the positive electrode. KCl precipitation in experimental cells may be a capacity-limiting mechanism; however, it appears to limit utilization at a much larger depth of discharge, if at all.

The main failure mechanism in experimental cells is the expansion and extrusion of active material, which eventually leads to short circuit. Positive electrode expansion is a problem during the discharge of experimental cells; however, it may be responsible for

eliminating or lessening the KCl precipitation problem in these cells. Fabricating electrodes with larger initial porosities may help reduce the problem of electrode swelling. It has been proposed that assembling the positive electrode in the fully discharged state (Li_2S and Fe) will reduce electrode expansion and increase cell performance.[1] Our models predict that the KCl precipitation problem is lessened by increasing the initial porosity of the positive electrode.

Our mathematical models predict that increasing the initial porosity of the positive electrode increases the cell voltage; this is because the solid electrode material is taken to be more conductive than the electrolyte in the pores.

The thermodynamic analysis indicates that lower operating temperatures and LiCl concentrations will enhance the reactions involving J-phase. Decreasing cell operating temperature and LiCl concentration are also predicted to decrease positive-electrode utilization if KCl precipitation in the positive electrode is the capacity-limiting mechanism. The low electrode utilization observed in the discharge of experimental cells with the J-phase mechanism may be due in part to the detrimental effects of KCl precipitation (which can be present at low operating temperature or high KCl concentrations).

The exchange current densities and transfer coefficients for all the electrode reactions and all of the properties of J-phase used in the models are not based on experimental data. There is a great need for the determination of kinetic data for the reactions as well as physico-chemical properties of the electrode phases in the modeling of the iron sulfide electrodes.

Acknowledgment

List of Symbols

a	interfacial area per unit electrode volume, cm^{-1}
a_i	activity of species i
a_l	constant in the expression for the open circuit potential of reaction l, V
b_l	temperature coefficient in the expression for the open circuit potential of reaction l, V/K
e^-	symbol for an electron
F	Faraday's constant, 96,487 C/equiv
i	current density, A/cm^2
$i_{o,l}$	exchange current density for reaction l, A/cm^2
i_l	partial current density of electrode reaction l, A/cm^2
L	length of cell, cm
m	precipitation parameter
n	number of discharge-charge cycles
n_e	number of moles of electrolyte per mole of FeS
n_l	number of electrons involved in reaction l

n_{RE} number of electrons involved in the reference electrode reaction

Q capacity per unit volume of electrode, C/cm^3

R universal gas constant, 8.3143 J/mol-K

$s_{i,l}$ stoichiometric coefficient of species i in reaction l

t time, s

T absolute temperature, K

U_l theoretical open-circuit potential for reaction l relative to a reference electrode, V

U_l^o standard electrode potential for reaction l, V

U_{RE}^o standard electrode potential for the reference electrode reaction, V

V cell potential, V

$x_{i,j}$ mole fraction of species i in phase j

y distance from electrode, cm

Greek letters

ϵ porosity or electrolyte volume fraction

ϵ_i volume fraction of species i

$\gamma_{i,j}$ activity coefficient of species i in phase j

Subscripts

A ambient

$continuous$ refers to phases that form a continuum

ccp current collector in the positive electrode

e electrolyte

eff	effective
i	refers to a species
l	refers to a reaction
matrix	refers to the solid electrode matrix
p	precipitate
pore	refers to the pores of an electrode
rev	reversible
RE	reference electrode reaction
s	refers to solid, surface, or separator
tot	total
+	positive electrode
−	negative electrode

Superscripts

eut	eutectic composition
final	at end of discharge
o	refers to secondary reference state or initial
RE	reference electrode composition

References

1. E. C. Gay, R. K. Steunenberg, W. E. Miller, J. E. Battles, T. D. Kaun, F. J. Martino, J. A. Smaga, and A. A. Chilenskas, in *Li-Alloy/FeS Cell Design and Analysis Report*, Argonne National Laboratory Report ANL-84-93 (July, 1985).

2. J. R. Selman, "Molten-Salt Battery Cells with Sulfur or Metal Sulfide Electrodes," R. P. Tischer, ed., *The Sulfur Electrode*, Academic Press, New York, pp. 219-232 (1983).

3. J. R. Selman and M. L. Saboungi, "Electrochemistry of Sulfur in Halide Melts," R. P. Tischer, ed., *The Sulfur Electrode*, Academic Press, New York, pp. 113-127 (1983).

4. R. Pollard, *Mathematical Modeling of the Lithium-Aluminum, Iron Sulfide Battery*, Dissertation, University of California, Berkeley (1979).

5. R. Pollard and J. Newman, "Mathematical Modeling of the Lithium-Aluminum, Iron Sulfide Battery. I. Galvanostatic Discharge Behavior," *Journal of the Electrochemical Society*, **128**, 491-502 (March, 1981).

6. R. Pollard and J. Newman, "Mathematical Modeling of the Lithium-Aluminum, Iron Sulfide Battery. II. The Influence of Relaxation Time on the Charging Characteristics," *Journal of the Electrochemical Society*, **128**, 503-507 (March, 1981).

7. C. E. Vallet, D. E. Heatherly, L. Heatherly, Jr., and J. Braunstein, "LiCl Precipitation from LiCl-KCl Anolyte in Porous Li-Al Electrodes," *Physical Chemistry of Molten Salt Batteries, Final Report for Period Oct. 1, 1981-Sept. 30, 1982*, Oak Ridge National Laboratory Report ORNL/TM-8714 (May, 1983).

8. C. E. Vallet, Personal Communication (1983).

9. Z. Tomczuk, S. K. Preto, and M. F. Roche, "Reactions of FeS Electrodes in LiCl-KCl Electrolyte," *Journal of the Electrochemical Society,* **128**, 760-772 (April, 1981).

10. Z. Tomczuk, M. F. Roche, and D. R. Vissers, "Emf Measurements on the Li-Al/FeS Couple in LiF-LiCl-LiBr Electrolyte," *Journal of the Electrochemical Society,* **128**, 2255-2256 (October, 1981).

11. J. Lumsden, *Thermodynamics of Molten Salt Mixtures,* Academic Press, New York (1966).

12. D. M. Bernardi, *Mathematical Modeling of Lithium(alloy),Iron Sulfide Cells and the Electrochemical Precipitation of Nickel Hydroxide,* Dissertation, University of California, Berkeley (1986).

13. D. M. Chen and H. F. Gibbard, "Thermal Energy Generation of LiAl/FeS Cells," *Journal of the Electrochemical Society,* **130**, 1975-1979 (October, 1983).

14. J. Newman, *Electrochemical Systems,* Prentice Hall, Englewood Cliffs, New Jersey (1973).

15. D. Bernardi, E. Pawlikowski, and J. Newman, "A General Energy Balance for Battery Systems," *Journal of the Electrochemical Society,* **132**, 5-12 (January, 1985).

16. D. Bernardi and J. Newman, "Mathematical Modeling of Lithium(alloy), Iron Disulfide Cells," submitted to the *Journal of the Electrochemical Society.*

17. S. P. S. Badwal and R. J. Thorn, "Conductivities and Electronic Structures of Some Phases in the Lithium-Iron-Sulfur System," *Journal of Solid State Chemistry ,* **43**,

163-174 (July, 1982).

18. R. E. Meredith and C. W. Tobias, "Conduction in Heterogeneous Systems," *Advances in Electrochemistry and Electrochemical Engineering 2,* C. W. Tobias, ed., Interscience Publishers, New York, pp. 15-47 (1962).

19. R. C. Elliott and T. O. Cooper, in *High Performance Batteries for Off-Peak Energy Storage and Electric-Vehicle Propulsion,* Argonne National Laboratory Report ANL-75-1, pages 25-29 (July, 1975).

Figure Captions

Figure 1. Reaction regions as a function of temperature and utilization for a cell with $x^0_{LiCl} = 0.58$ and $n^0_e = 1.0$. The numbers refer to the reactions in Table 1, and parentheses indicate a reaction that can be obtained from the other two reactions.

Figure 2. The open-circuit potential behavior as a function of temperature at different percent utilization for a cell with $x^0_{LiCl} = 0.58$ and $n^0_e = 1.0$.

Figure 3. Calculated open-circuit potential behavior as a function of temperature at different percent utilizations for a cell with $x^0_{LiCl} = 0.58$ and $n^0_e = 2.55$.

Figure 4. Schematic diagram of the LiAl/FeS cell.

Figure 5. Position dependence of the mole fraction of LiCl at different states of discharge for the J-phase mechanism. Simulation parameters are for the base case (Tables 2 and 3).

Figure 6. Cell voltage as a function of positive electrode utilization for the J-phase mechanism for two values of m and ϵ^0_+. Simulation parameters are for the base case except m and ϵ^0_+.

Figure 7. Experimental cell voltage as a function of positive electrode utilization at 443°C using electrolyte of eutectic composition.[9]

Figure 8. Maximum positive electrode utilization as a function of ϵ_+^o. The points are simulation results.

Figure 9. Average positive-electrode expansion of a series of experimental cells as a function of state-of-charge.[1]